Glass Ceramic Waste Forms for Combined CS+LN+TM Fission Products Waste Streams

Fuel Cycle Research & Development

Prepared for
U.S. Department of Energy
Waste Form Campaign
J.V. Crum, L.R. Turo, and B.J. Riley
Pacific Northwest National Laboratories
M. Tang, A. Kossoy, and K.E. Sickafus
Los Alamos National Laboratories

September 24, 2010
FCRD-WAST-2010-000181
PNNL-19780

SUMMARY

In this study, glass ceramics were explored as an alternative waste form for glass, the current baseline, to be used for immobilizing alkaline/alkaline earth + lanthanide (CS+LN) or CS+LN+transition metal (TM) fission-product waste streams generated by a uranium extraction ($UREX^+$) aqueous separations type process. Results from past work on a glass waste form for the combined CS+LN waste streams showed that, as waste loading increased, large fractions of crystalline phases precipitated upon slow cooling.[1] The crystalline phases had no noticeable impact on the waste form performance by the 7-day product consistency test (PCT).[1] These results point towards the development of a glass ceramic waste form for treating CS+LN or CS+LN+TM combined waste streams. Three main benefits for exploring glass ceramics are:

- Glass ceramics offer increased solubility of troublesome components in crystalline phases as compared to glass, leading to increased waste loading.
- The crystalline network formed in the glass ceramic results in higher heat tolerance than glass.
- These glass ceramics are designed to be processed with the same melter technology as the current baseline glass waste form. It only requires controlled canister cooling for crystallization into a glass ceramic waste form.
- Highly annealed waste form (essentially crack free) with up to 50X lower surface area than a typical high-level waste (HLW) glass canister. Lower surface area translates directly into increased durability.

The work reported here has shown that dramatic increases in waste loading are achievable by designing a glass ceramic waste form as an alternative to glass. Table S1 shows the upper limits for heat, waste loading (based on solubility), and the decay time needed before treatment can occur for glass and glass ceramic waste forms. The improvements are significant for both combined waste stream options in terms of waste loading and/or decay time required before treatment. For Option 1, glass ceramics show a potential increase in waste loading of 15 mass% and reduction in fuel storage time (decay time) of 24 years. Decay times of ~50 years or longer are close to the expected age of the fuel that will be reprocessed when the modified open or closed fuel cycle is expected to be put into action. Option 2 shows a 2× to 2.5× increase in waste loading with decay times of only 45 years. For the Option 2 glass, the required decay time before treatment is only 35 years because the waste loading limits are related to the low solubility of MoO_3 in glass. If glass was evaluated for similar waste loadings as those achieved in Option 2 glass ceramics, the decay time would be significantly longer than 45 years. These glass ceramics are not optimized, but already they show the potential to dramatically reduce the amount of waste generated while still utilizing the proven processing technology used for glass production.

For the radiation stability test, selected glass ceramic samples were exposed to either low fluxes of high-energy (~3-5 MeV) protons and alphas, or in-situ electron irradiations in a transmission electron microscope. The preliminary XRD and TEM results show the very good radiation tolerance, especially the amorphization resistance, in our glass ceramics. Additional study to probe atomic and microstructural evolution of individual crystalline phases under irradiation is needed in the future.

Table S1. Comparison of baseline glasses to current glass ceramic waste forms

Option 1	Glass [1]	Glass Ceramic	
Heat Limit, °C	700	1250	1250
Waste Loading, %	45	55	60
Required Decay, y	76	48	52

Option 2	Glass [1]	Glass Ceramic	
Heat Limit, °C	500	950	950
Waste Loading, %	20	40	50
Required Decay, y	35	36	45

Option 1 = CS+LN, Option 2 = CS+LN+TM

The FY 2010 scope was to explore silicate-based glass ceramics for immobilizing Option 1 and 2 combined waste streams and to show that glass ceramics can present a very viable treatment option in terms of waste form volume and overall cost. The FY 2011 efforts will focus on the further development of Option 2 glass ceramics, which offers the possibility of treating all three waste steams into in a single waste form. From a reprocessing operations standpoint, this would be the simplest and most cost effective immobilization option. Specifically, the following questions and tasks will be addressed:

- Full chemical and structural characterization of multiphase glass ceramics, including techniques such as focused ion beam-transmission electron microscopy (FIB-TEM), synchrotron diffraction, electron microprobe, and micro X-ray diffraction (XRD).
    - TEM will be used to provide more complete analyses of the ~1μm powellite crystals.
    - Electron microprobe will provide accurate compositions of the larger scale crystalline phases.
    - Synchrotron diffraction will be used to obtain high quality diffraction patterns of the complex multiphase glass ceramics.
- Evaluate performance of the multi-phase glass ceramics with static and flow-though dissolution tests.
- Reformulate glass ceramics to improve performance and waste loading.

The following optional tasks will be pursued if time and budget allow:

- Synthesize powellite, oxyapatite, and rare earth (RE)-borosilicate crystalline phases for radiation damage testing at Los Alamos National Laboratory.
- Evaluate the performance of individual crystalline phases with dissolution tests.
- Identify and test a method for irradiation of a glass ceramic on a large enough scale for dissolution testing, followed by static or flow through dissolution testing.

CONTENTS

FIGURES

TABLES

ACRONYMS

AFCI	Advanced Fuel Cycle Initiative
BSE	back-scattered electron
CS	alkaline/alkaline earth fission products
DOE	U.S. Department of Energy
EDS	energy dispersive spectroscopy
EELS	electron energy loss spectroscopy
EML	Electron Microscope Laboratory
FFT	Fourier transforms
FIB	focused ion beam
HLW	high-level waste
IBML	Ion Beam Materials Laboratory
ICCD	International Center of Crystallographic Data
ICSD	International Center of Structure Data
LANL	Los Alamos National Lab
LN	lanthanide fission products
LVDT	linear variable differential transformer
NIST	National Institute of Standards and Technology
OM	optical microscope(y)
Option 1	CS + LN combined waste stream
Option 2	CS + LN + TM combined waste stream
PCT	product consistency test
PDF-2	Powder Diffraction File
PNNL	Pacific Northwest National Laboratory
PSD	position sensitive detector
RT	room temperature
RE	rare earth
RO	alkaline earth oxide
R_2O	alkali oxide
SEI	secondary electron image
SEM	scanning electron microscope(y)
SLR	single lens reflex
SRIM	the stopping and range of ions in matter
SRM	standard reference material

SUTW	super ultra thin window
T_d	dilatometric softening point
TEM	transmission electron microscopy
T_g	glass transition temperature
T_M	glass melting temperature
TM	transition metal fission products
UREX$^+$	uranium extraction process
XRD	X-ray diffraction

WASTE FORMS CAMPAIGN/FCR&D PROGRAM

1. INTRODUCTION

Borosilicate glass was selected as the baseline technology for treating the alkaline/alkaline earth (CS), lanthanide (LN), and transition metal (TM) fission-product waste streams generated by the uranium extraction (UREX$^+$) separations process.[2] In FY2009, high degrees of crystallization were observed in glasses with high waste loading upon slow cooling without any significant change in waste form performance as measured with the product consistency test (PCT).[1] Those results showed the possibility of developing a glass ceramic that takes advantage of crystallinity instead of the long-standing approach to avoid crystallinity in glass. The presence of crystallinity could lead to higher waste loadings than in a completely vitreous glass; however, the crystalline phase types formed could deplete the remaining glass of glass formers, resulting in a less durable glass phase. For this reason, crystalline phases have generally been avoided in developing borosilicate glass waste forms for high-level waste (HLW) with the main focus on avoiding silicates, such as nepheline.[3-5] For the glasses developed in FY2009, the glass phase remained durable upon crystallization, indicating that the composition space investigated is more accommodating to a glass ceramic approach.

The main reasons to develop a glass ceramic instead of a glass are:

1) Higher waste loading by increased solubility of troublesome components in crystalline phases.
2) Higher heat tolerance by eliminating T_g constraint and elevating it to the lowest crystalline phases T_M.
3) Elimination of cracking during waste form synthesis, leading to a much greater overall durability
4) Process via melt process using baseline melter technology (cold crucible melter).

Alkali, alkaline earths, lanthanides, and especially MoO_3 each exceed the solubility limits of a single phase glass waste form upon slow cooling; however, they all dissolve at high temperature and form molten glass that can be processed with the baseline melter technology. Upon pouring into a canister, the cooling profile of the canister can be controlled to transform the glass to a glass ceramic.

For these reasons, a scoping study was started late in FY2009 to evaluate a glass ceramic approach for the CS + LN waste streams.[6] The results of the scoping studies showed that the glass system could easily be tailored into a multi-phase glass ceramic with the following crystalline phases: pollucite ($CsAlSi_2O_6$), celsian ($Ba_xSr_{(1-x)}Al_2Si_2O_8$), and oxyapatite ($Sr_xNd_{(10-x)}Si_6O_{26}$). These phases as a whole accommodate all of the major waste components present in the CS and LN fission-product waste streams.

Our FY2010 efforts focused on further examination of the combined CS+LN (Option 1) as well as expanding the glass ceramic concept to the combined CS+LN+TM fission products (Option 2). For Option 2 glass ceramics, the solubility of MoO_3, which phase separates upon cooling into a separate Mo-rich liquid phase, is problematic. The Mo-rich liquid phase then crystallizes upon further cooling into powellite ($XMoO_4$) where X is a combination of alkaline earths, alkali, and lanthanides. The durability of alkaline earth and lanthanide rich powellite is quite good, where as alkali rich powellite is poor. Thus, composition of powellite is tailored to minimize the inclusion of alkali. Celsian and oxyapatite also crystallize in the Option 2 glasses, similar to Option 1.

Two parameters were changed to achieve a glass ceramic instead of a glass waste form: chemistry and heat-treatment. The SiO_2, Al_2O_3, B_2O_3, and CaO concentrations and waste loading were varied to achieve a glass melt with a higher propensity to crystallize compared to the glass formulations investigated in FY2009.[1] Lime (CaO) was used in Option 2 glasses only to influence the formation and chemistry of the powellite phase.

The glasses were either, quenched and reheated, or they were slow cooled from the melt temperature to form a glass ceramic. Ideally, the cost is lowest if glass ceramics can be produced by controlling the cooling process. Reheating the glass to grow crystalline phases leads to increased cost and further engineering.

2. METHODS

2.1 Glass Ceramic Fabrication

The glass ceramics were batched from oxides, carbonates, boric acid, and Ru-nitrate in solution.[7] Ruthenium oxide was added to Option 1 glass only in the form of Ru-nitrate dissolved in water to ensure intimate mixing with the dry chemicals during the batching process. Once the Ru-nitrate solution dried onto the batch materials, the batch was mixed in an agate milling chamber for 4 minutes. The glasses were melted between 1200°C and 1600°C for 1 hour and cast onto a steel plate. The quenched glass was ground in a tungsten carbide milling chamber for 4 minutes to re-homogenize chemically for any heavy elemental segregation during the first melt, and then it was remelted for 1 hour and quenched on a stainless steel plate.

2.1.1 2-Step Heat Treatment (reheat process)

Glass samples were loaded into platinum boats with tight fitting lids and then heat treated at 950°C for 1 hour to nucleate crystals followed by a 3°C/min ramp to the crystal growth temperature of 1250°C and held for 4 hours. The samples were then cooled at 3°C/min to room temperature. This heat treatment was selected to allow crystallization of pollucite, celsian, and RE-apatite.

2.1.2 Controlled Cool Heat Treatment

Glass ceramics were also formed by a controlled cooling schedule. Samples were loaded into platinum boats with tight-fitting lids and placed in a furnace at the melting temperature. Then the furnace was cooled down to room temperature according to the calculated slow-cooling profile for the Option 1 glasses.[1] Alternatively, glasses were cooled from the melting temperature to room temperature at a rate of 3°C/min.

2.2 Characterization

The glass ceramics were characterized with several methods to determine the phase assemblage and morphology of the waste forms. First, a thin section was cut vertically through the glass ceramic to examine the crystallization behavior at the boundaries and in bulk by optical microscopy (OM) and scanning electron microscopy (SEM). Second, a representative sample was taken from the bulk and powdered for X-ray diffraction (XRD). Lastly, a bar was cut from the bulk for dilatometer measurements. Details of each technique are given below.

2.2.1 Optical Microscopy

Optical microscopy (OM) was done on polished cross-sections with reflected polarized light and cross-polarized light. The OM used for these tests is a Leitz Orthoplan with a magnification range of 15×-500×. Pictures were taken with a Canon Rebel single lens reflex (SLR) adapted to the microscope. Scaling added by processing software was calibrated by taking pictures of a ruler at each magnification.

2.2.2 SEM/EDS

Polished cross-sections were sputter coated with palladium and then loaded into the SEM to examine the morphology and elemental chemistry of the crystalline phases. The SEM is a JEOL 5900 with a tungsten wire filament. It is equipped with an energy dispersive spectroscopy (EDS) system for elemental analysis. The EDS detector is a Li drifted silicon detector cooled by liquid nitrogen with a super ultra thin window (SUTW), manufactured by EDAX.

2.2.3 XRD

Samples were spiked with a known concentration of an internal standard and powdered in a tungsten carbide milling chamber. Then they were pressed into a standard 25-mm-diameter powder mount. The powder mount was then loaded into a Bruker D8 advanced diffractometer. The D8 has a Cu X-ray target, a goniometer radius of 250 mm, a 0.3° fixed divergence slit, and a LynxEye position sensitive detector (PSD) with an angular range of 3°. Scan parameters are as follows: range 5 to 70° 2θ, step size 0.015° 2θ, and a hold time of 0.3 s/step. Crystalline phases were identified with Jade 6.0 software equipped with both the International Center of Crystallographic Data (ICCD) PDF2 release 1999 and the International Center of Structure Data (ICSD) release 2004. Whole pattern fitting was done using TOPAS 4.2 software to determine the quantitative fractions of the crystalline phases. Fitting was done using the fundamental parameters approach described by Cheary et al.[8]

2.2.4 Dilatometry

Expansion was measured as a function of temperature for a heating rate of 2°C/min up to 1000°C, which is the max temperature for the dilatometer system. The dilatometer provides a method for measuring expansion, T_g, and T_d (dilatometric softening point).

A bar with the approximant dimensions of 6 mm W × 6 mm D × 25.4 mm L were cut with parallel ends on a low-speed saw with a diamond-impregnated wafer blade. Cutting was done wet with water lubricant. Next, the bar was loaded into Dilatronic II, manufactured by Theta Industries, equipped with a single push rod and fused quartz sample holder. The measuring head is a digital linear variable differential transformer (LVDT). The LVDT was calibrated using a micrometer and verified by measuring with a NIST SRM 732 single crystal sapphire rod.

2.2.5 TEM

Sample was prepared in plan-view geometry for TEM examination. Final thinning to electron transparency was accomplished using 4 keV Ar^+ ion milling. Microstructure and elemental chemistry of the crystalline phases in GC-4 sample were examined using a FEI Tecnai F30 electron microscope operating at 300 kV in the Electron Microscope Laboratory (EML) at LANL.

2.2.6 Ion Beam Irradiation

Preliminary evaluations of the radiation damage tolerance of the glass ceramic waste forms were performed at LANL. Protons (H^+), Helium (He^+), and electrons (e^-) were used to simulate the self-radiation damage that occurs in a material incorporating nuclides that are undergoing radioactive decay. Most of the self-irradiation in a waste form incorporating FPs is due to beta (β) particle and gamma (γ) emission. These emissions cause radiation damage primarily via radiolytic processes, both β and γ particles induce substantial electronic excitations in a target material. However, β and γ particles are only partially attenuated by the surrounding waste form, a significant fraction the energy may escape. Proton, alpha, and electron particles provide a useful means to examine radiolysis effects, because they deposit nearly all of their energy in solids via electronic loss processes(electronic-to-nuclear stopping power ratio of nearly 2000 for 3 MeV H^+ in SiO_2). As such, these tests provide an upper bound for the β and γ emissions in the waste form.

In these experiments, we irradiated GC-4 and Mo-6.94% samples in the Ion Beam Materials Laboratory (IBML) at Los Alamos, with 3 MeV H^+ and 5 MeV He^+ ions generated in a 3.2 MV tandem ion accelerator with the samples at two temperatures: (1) room temperature (25°C), and (2) 230°C. The elevated temperature served to simulate decay heats representative of different radionuclide loadings of a waste form. For the electron beam irradiation study, a TEM specimen was prepared in plan-view geometry. This plan-view sample was examined at room temperature in a FEI Tecnai F30 electron microscope operating at 300 kV. Electron irradiation experiments were carried out by focusing the electron beam onto small regions of electron transparent material (a typical irradiated region was ~100 nm diameter).

3. Glass Formulation

3.1.1.1 Option 1

Two compositions were selected near compositions of the highly crystallized glasses from the FY2008 and FY2009 glass development work, with target compositions shown in Table 1.[1,9] The additives, Al_2O_3 and SiO_2, were chosen for target crystalline phases—oxyapatite, celsian, and pollucite—and B_2O_3 was selected to lower the $T_M \leq 1600$°C. A trace amount of RuO_2 was added to the batches to provide nucleation sites for crystalline phase formation upon heat treatment or controlled cooling. Sample GC-10B was the first attempt to transition from a glass formulation to a glass ceramic. The waste loading was 5 mass% higher than the Option 1 baseline glass.[1] Sample GC-4 was formulated based on the results obtained from GC-10B to crystallize more rapidly upon cooling, avoiding a heat-treatment step. Waste loading was increased to 60 mass% at the expense of Al_2O_3 and SiO_2. Boron trioxide was increased in GC-4 to offset the increased waste loading and maintain the $T_M \leq 1600$°C.

3.1.1.2 Option 2

Three compositions were formulated for the Option 2 glass ceramics with waste loadings of 42 mass%, 45 mass%, and 50 mass% with target compositions given in Table 1. The Option 2 glasses were formulated to form similar crystalline phases—oxyapatite, celsian, and pollucite—as the Option 1 glasses plus powellite for the high MoO_3 in the Option 2 combined waste stream. Past glass formulation work by Crum et al.[1] showed that only ~2.5 mass% MoO_3 was soluble in the baseline borosilicate glass network. The additives chosen for Option 2 glasses were the same as Option 1 plus the use of CaO to aid the formation of powellite, rich in alkaline earths and lanthanides. The molar ratios were fixed for all three formulations at CaO/alkali = 1.75 and B_2O_3/alkali = 1.75, based on the results of a study by Caurant et al.[10] An abundance of alkaline earths and lanthanides is needed to avoid the formation of alkali rich molybdates, which are less durable. The alkaline earths and lanthanides were expected to combine with Mo and precipitate out of the glass melt at higher temperatures, thus consuming the Mo before the alkali molybdates can precipitate.

Table 1. Target Compositions for Option 1 and 2 glass ceramics

Option	1	1	1	1	2	2	2	2	2	2
ID	10B	10B	4	4	Mo-5.86	Mo-5.86	Mo-6.25	Mo-6.25	Mo-6.94	Mo-6.94
	mass%	mole%	mass%	mole%	mass%	mole%	mass%	mole%	mass%	mole%
Al_2O_3	17	18.8	8	14.5	6	5.3	5	4.5	5	4.8
B_2O_3	10	16.2	15.3	19	9.5	12.3	9.4	12.5	8.4	11.7
SiO_2	23	43.1	17.8	37.4	34.8	52.1	32.8	50.4	29	47
MoO_3	0	0	0	0	5.8	3.7	6.3	4	6.9	4.7
RO	8.5	7	10.1	9.3	8.7	9.6	9.4	10.5	10.4	12.3
R_2O	7.5	3.2	8.8	4.2	8.6	7	8.8	7.12	8.7	6.7
LN_2O_3	34	11.7	39.9	15.5	20	5.5	21.4	6.1	23.8	7.1
ZrO_2	0	0	0	0	4.5	3.3	4.8	3.6	5.3	4.2
Others	0	0	0	0	2	1.2	2.1	1.3	2.4	1.5
RuO_2^*	0.05	0.04	0.1	0.1						
Total	100	100	100	100	100	100	100	100	100	100
Waste Loading	50		60		42		45		50	

RO = sum of alkaline earth oxides, R_2O = sum of alkali oxides, others = sum of PdO, RhO_2, RuO_2, Ag_2O, CdO, Sb_2O_3, SeO_2, SnO_2, and TeO_2, * RuO_2 added as nucleation agent

4. Results

4.1.1 Melt Observations before Crystal Growth

4.1.1.1 Option 1 Glasses

Glasses were air quenched on a stainless steel plate after melting. Sample GC-10-B contained only a few crystals when air quenched from the melting temperature. The viscosity of GC-10-B was visually approximated to be less than 10 Pa·s. Sample GC-4, on the other hand, contained a significant fraction of crystals upon air quenching from a melt. The viscosity of GC-4 also appeared to be near or slightly above 10 Pa·s at the melting temperature, based on visual observations.

4.1.1.2 Option 2 Glasses

All of the Option 2 glasses appeared opaque upon air quenching, indicating liquid or crystalline phase separation upon quenching from a melt. The viscosity was visually estimated to be within a range of 2 to 10 Pa·s, the typical operation range for most glass melter processes.

4.1.2 Optical Microscopy and SEM/EDS of Glass Ceramics

4.1.2.1 Option 1 Glasses

SEM micrographs show the glass ceramics are highly crystallized with varying amounts of glass phase remaining. Sample GC-10-B contains three crystalline phases after heat treatment to 950°C for 1 hour,

followed by a 3°C/min ramp to 1250°C and a hold of 1 hour, shown in Figure 1. In Figure 1D (BSE image) the large crystals (white in the photomicrograph) are lanthanide rich oxyapatite, the crystals (black) are celsian, and the ill-defined crystal shapes (dark grey) are pollucite. There is a remaining glass network that makes up the background or matrix of the images. The glass fraction remains at a high enough concentration to be connected in most areas of the sample. The elemental composition of each phase found in sample GC-10B was measured with EDS, and they are given in Table 2 and Table 3 in terms of mass% and mole %. Boron cannot be detected with the EDS detector, so there is a possibility that boron is present in some or all of the phases. We used the XRD results, Section 4.1.3, to confirm the presence of boron. There is an alkali-alumino-silicate phase (pollucite), alkaline earth-alumino-silicate phase (celsian), rare earth-silicate phase (oxyapatite), and a glass matrix. The glass composition is dominated by SiO_2, Al_2O_3, and rare earth oxides.

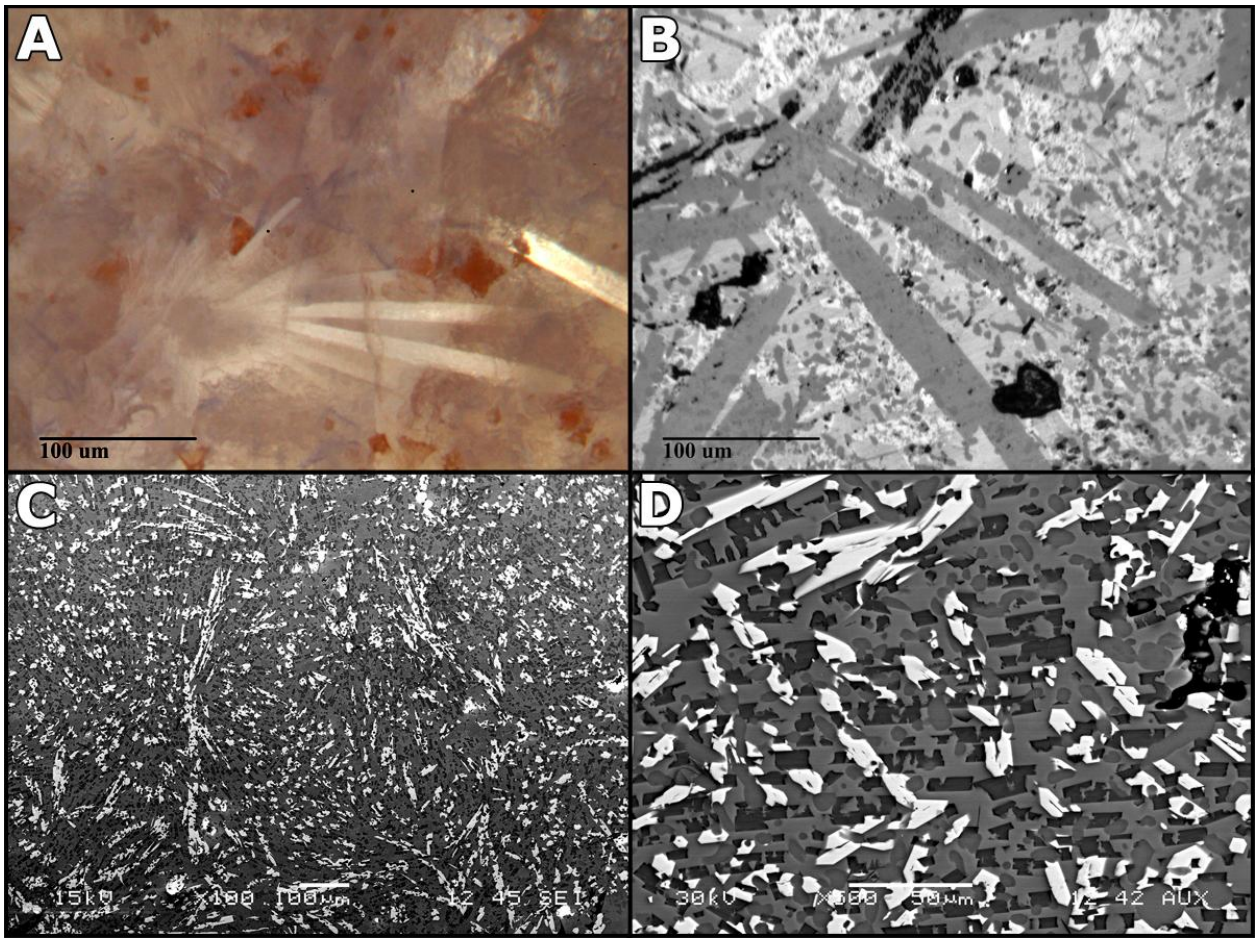

Figure 1. OM and SEM micrographs of GC-10B after two-step heat treatment (950°C-1 hour, 3°C/min ramp to 1250°C-4 hours). A) 200× polarized light OM, B) 200× reflected light OM, C) 100× (SEI), and D) 500× back-scattered electron (BSE).

Table 2. EDS measured elemental compositions for crystalline phases in GC-10B

Filename	units	O	Al	Si	Sr	Y	Cs	Ba	La	Ce	Pr	Nd	Total
Ba-Al-Silicate	Mass%	13	18	19	11	0	0	39	0	0	0	0	100
Cs-Silicate	Mass%	11	12	27	0	0	45	5	0	0	0	0	100
Re-Silicate	Mass%	8	0	12	0	4	0	0	10	16	7	42	100
Ba-Al-Silicate	Mole%	32	26	27	5	0	0	11	0	0	0	0	100
Cs-Silicate	Mole%	28	18	39	0	0	14	2	0	0	0	0	100
Re-Silicate	Mole%	33	1	27	0	3	0	0	5	8	3	19	100

Table 3. EDS measured elemental compositions for glass phase in GC-10B

Filename	Units	Al_2O_3	SiO_2	Y_2O_3	Cs_2O	La_2O_3	Ce_2O_3	Pr_2O_3	Nd_2O_3	Total
Glass	Mass%	23	22	3	1	7	14	5	25	100
Glass	Mole%	29	48	2	0	3	5	2	10	100

The SEM micrographs of sample GC-4 are shown in Figure 2. The crystalline phases in sample GC-4 are similar to the crystalline phases observed in sample GC-10-B. However, there are two additional phases in sample GC-4, lanthanide borosilicate and cerianite. Sample GC-4 also appears to have essentially converted to a ceramic upon cooling from 1600°C to room temperature (RT) at 3°C/min. The remaining glass phase is a very small fraction that is confined to the grain boundaries and is not visible in any of the SEM micrographs.

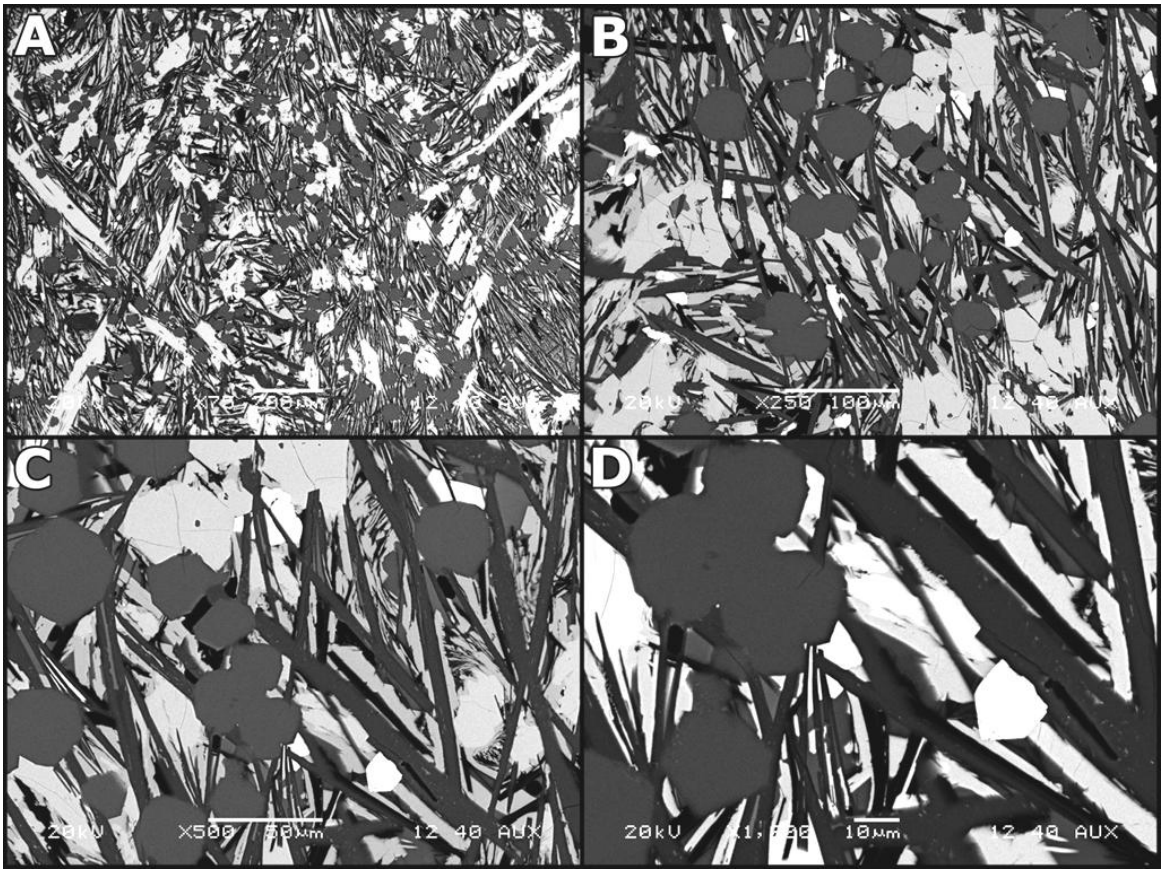

Figure 2. Back-scattered electron micrographs of sample GC-4 after 3°C/min cooling schedule from 1600°C to RT. A) 75×, B) 250×, C) 500×, and D) 1000×

An elemental dot map was collected on a cross section of the GC-4 sample after cooling at 3°C/min from 1600°C to RT, shown in Figure 3. The dot maps of the individual elements show that there are five oxide phases: Si-Ba-Al oxide, rare earth (RE)-Si-Al oxide, RE-Si oxide, Al-RE oxide, and lastly a Ce-O rich phase. Next, a cluster analysis was performed with the EDS analysis software to identify regions with similar yet distinct chemistry as well as determine the relative volume fractions of each phase in the image area with results shown in the legend attached to Figure 3. The cluster analysis was performed on the EDS spectrum collected at each pixel location of the elemental map, and it was compared to the 4×4 surround pixels. The phases were fine tuned by spot analysis of individual phases. On a volume basis, Ba-Al-Si-O is the most abundant phase, followed by RE-Al-Si-O, RE-Si-O, RE-Al-O, and Ce-O, respectively. The location of B could not be determined with this EDS detector. In addition, the cluster analysis was not useful in identifying a glass phase, but the scale of the glass phase is likely too small for it to be distinguished with the cluster analysis method.

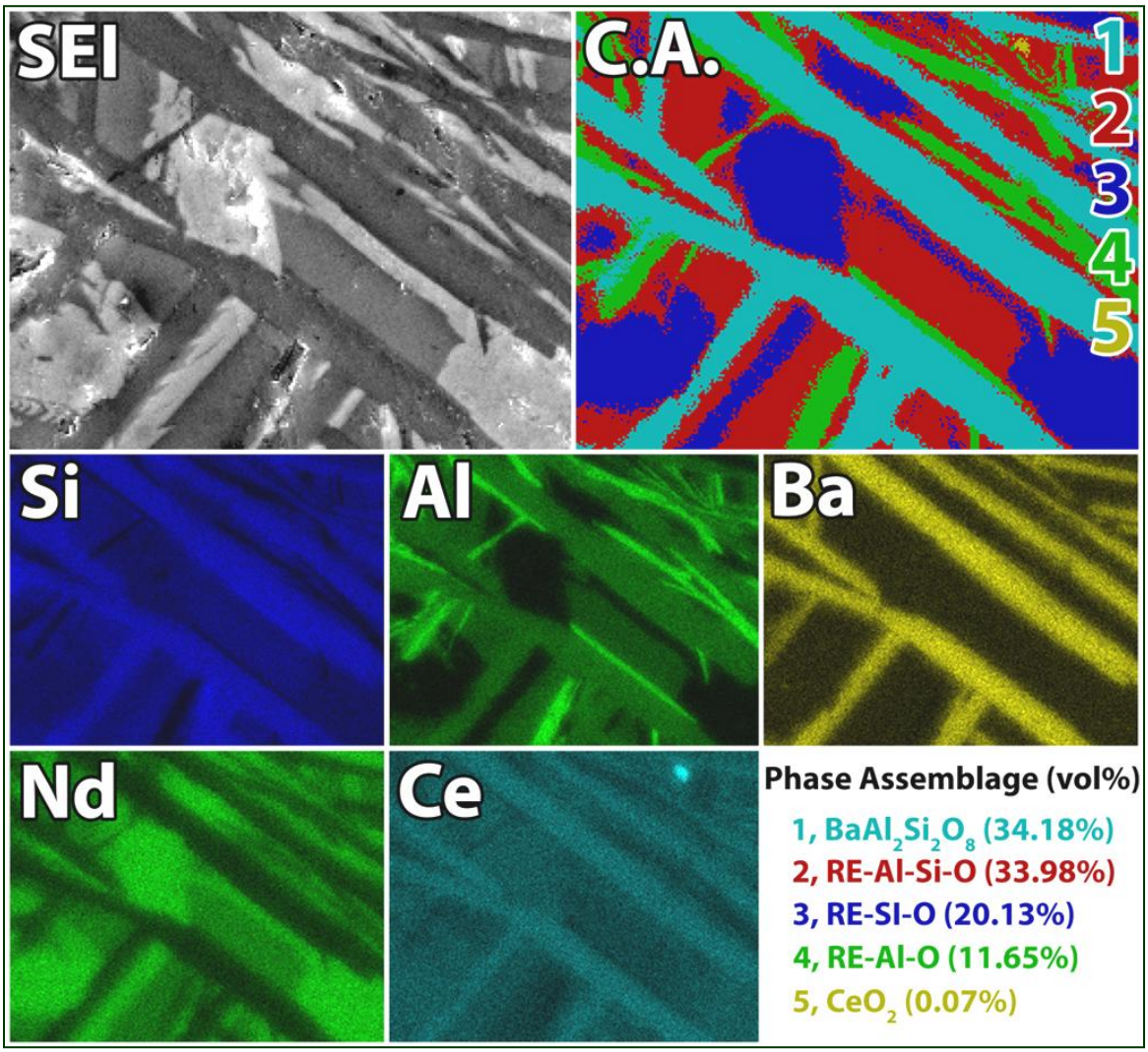

Figure 3. Sample GC-4 cooled 3°C/min from 1600°C to RT. Images include SEI, elemental maps, and cluster analysis with phases denoted in legend

4.1.2.2 Option 2

The SEM micrographs of the Option 2 glass ceramics after slow cooling heat treatment are given in Figure 4 through Figure 8. Figure 4 shows a montage of magnifications for sample GC-Mo-5.86. Large-

scale liquid phase separation is seen in Figure 4A, evidenced by the light-colored, irregular-shaped regions. Upon closer examination, both the light and dark regions have crystallized into three distinct crystal morphologies. In addition, there are 5-μm size, round, dark, non-crystalline regions that are apparent at 2500× in Figure 4E and F. The sample shows evidence of liquid phase separation on a large scale and micron scale as well. It appears the large-scale, liquid-phase separation later crystallized. Samples GC-Mo-6.25 and GC-Mo-6.94 are each shown with crystal orientation parallel and perpendicular in Figure 5 through Figure 8. As waste loading and MoO_3 concentrations increase, the large-scale phase separation ceases to be apparent. However, the micrometer-sized, dark silica-rich spots are apparent, and the crystalline phases remain similar for all waste loadings. The crystalline phases observed are similar to the Option 1 glasses plus the addition of the powellite phase.

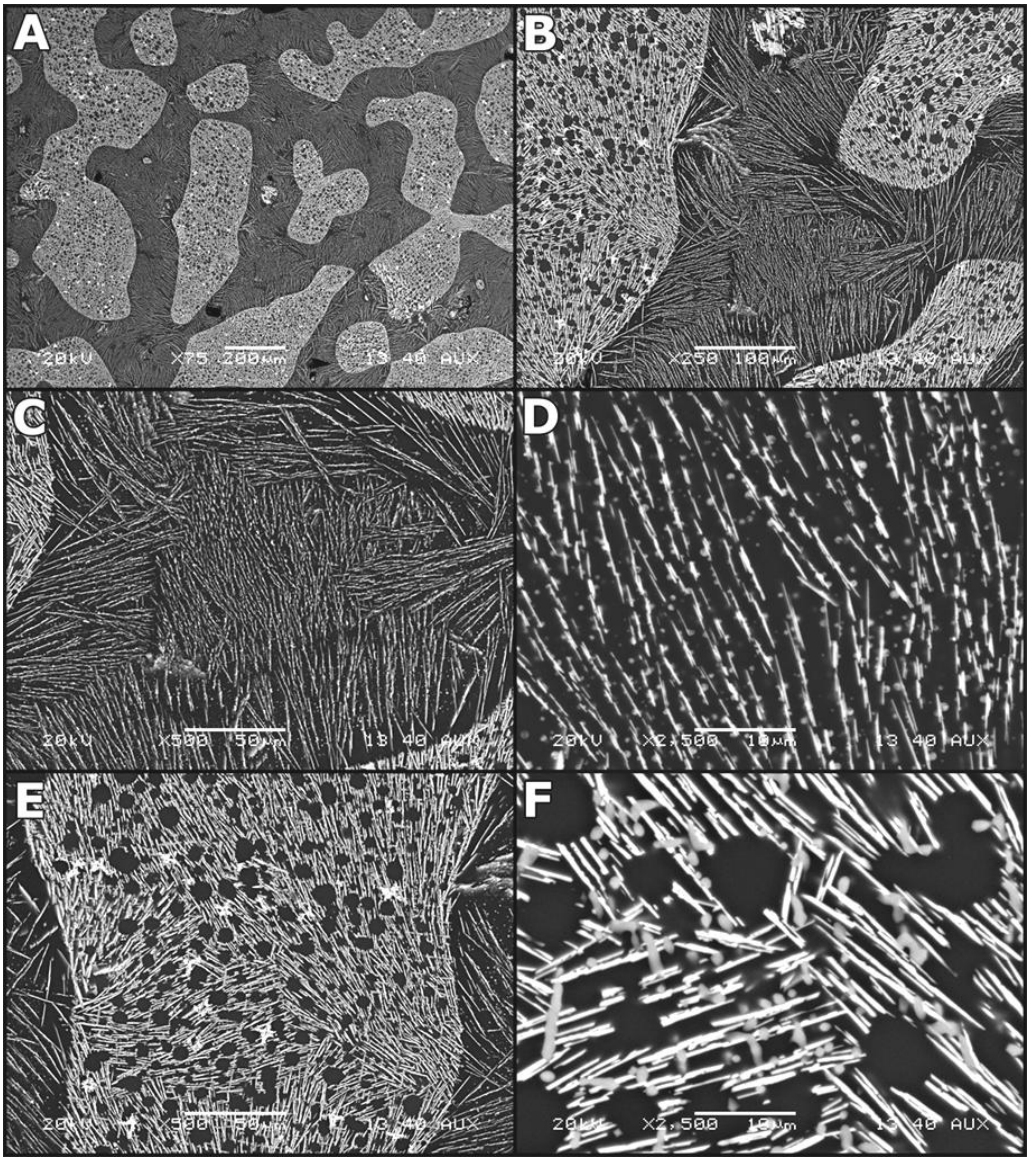

Figure 4. Back-scattered electron imaging micrographs of GC-Mo-5.86 (Option 2) glass ceramic after slow cooling treatment schedule

The crystals observed in the GC-Mo-5.86 sample, slow-cooled glass ceramic are too small to obtain accurate elemental analyses with EDS. As a result, elemental compositions are an average of the spot of

interest plus the glass matrix or crystals surrounding the spot of interest. Thus, the measured compositions are only useful to show relative changes to one another for this sample. Table 4 shows the measured compositions along with the associated crystal phase. The phases are based on XRD-identified phases.

Table 4. Elemental compositions determined form EDS spot analysis of sample GC-Mo-5.86 after slow-cooled heat treatment. Compositions are grouped based on morphology and chemistry.

Phase	O	Alkali	Alkaline earth	Mo	Zr	Si	Al	RE	Total
Oxyapatite	42	0	6	0	0	28	2	19	98
Oxyapatite	44	4	3	0	1	26	3	17	98
Oxyapatite	41	4	7	0	1	26	3	16	98
RE-borosilicate	73	1	4	2	0	11	1	6	100
RE-borosilicate	42	4	5	1	1	30	4	11	99
RE-borosilicate	44	3	5	0	1	25	2	18	98
RE-borosilicate	68	0	2	0	0	13	1	14	99
RE-borosilicate	69	0	2	0	0	13	0	13	99
Glass	44	7	4	0	2	33	9	1	100
Glass	43	8	3	1	1	36	8	1	100
Glass	47	6	4	0	2	34	8	0	100
Powellite	46	6	4	6	1	27	7	1	99
Powellite	43	4	16	19	1	7	1	9	99
Powellite	48	4	14	19	1	7	2	4	99
Powellite	40	4	17	22	1	9	2	5	99
Powellite	45	5	18	27	0	0	0	5	100
Powellite	49	4	17	27	0	0	0	3	100
Powellite	48	4	16	14	1	13	3	0	100
Powellite	76	2	8	7	0	6	1	0	100
Powellite	73	1	12	11	0	2	1	0	100
Powellite	49	5	11	12	1	15	3	4	100
Powellite	17	2	26	25	1	8	1	20	100
Cerianite	74	2	2	0	10	7	1	4	99

Elemental analysis results for samples GC-Mo-6.25 and GC-Mo-6.94 slow cooled are given in Table 5 and Table 6. Again, like sample GC-Mo-5.86, the crystals are too small to accurately measure the compositions by the EDS method. As such, the phases were determined based on XRD analysis, and the compositions are an average of the spot of interest plus the surrounding area. They are only useful to track the relative changes in composition. The measured compositions for the powellite phase are drastically affected by the surrounding glass. Elemental analysis was performed on oxyapatite and powellite in each of these samples; cerianite was also visually observed whereas RE-borosilicate was not.

Table 5. Elemental compositions determined from EDS spot analysis of sample GC-Mo-6.25 after slow cooled heat treatment. Compositions are grouped based on morphology and chemistry.

Phase	O	Alkali	Alkali Earth	Al	Si	Zr	Mo	RE	Total
Oxyapatite	55	0	6	0	19	0	0	20	100
Oxyapatite	56	3	4	3	21	1	1	11	100
Oxyapatite	55	2	3	1	19	1	0	19	100
Oxyapatite	50	1	6	1	21	0	0	20	100
Powellite	64	4	8	3	12	1	8	1	100
Powellite	61	3	9	2	12	1	9	2	100
Powellite	56	2	13	1	6	1	15	6	100

Table 6. Elemental compositions determined from EDS spot analysis of sample GC-Mo-6.94 after slow-cooled heat treatment. Compositions are grouped based on morphology and chemistry.

Phase	O	Alkali	Alkali Earth	Al	Si	Zr	Mo	RE	Total
Powellite	61	3	11	2	8	1	12	2	100
Oxyapatite	51	1	8	0	18	0	0	22	100

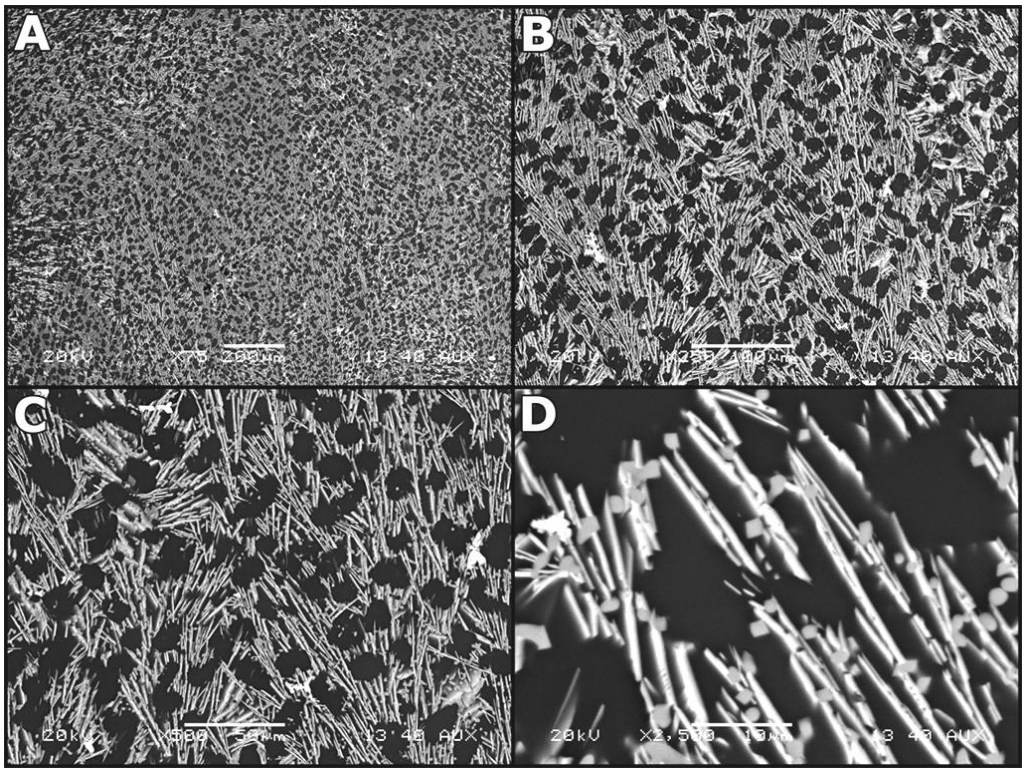

Figure 5. Back-scattered electron imaging micrographs of sample GC-Mo-6.25 (Option 2) glass ceramic with detail on crystals parallel to image

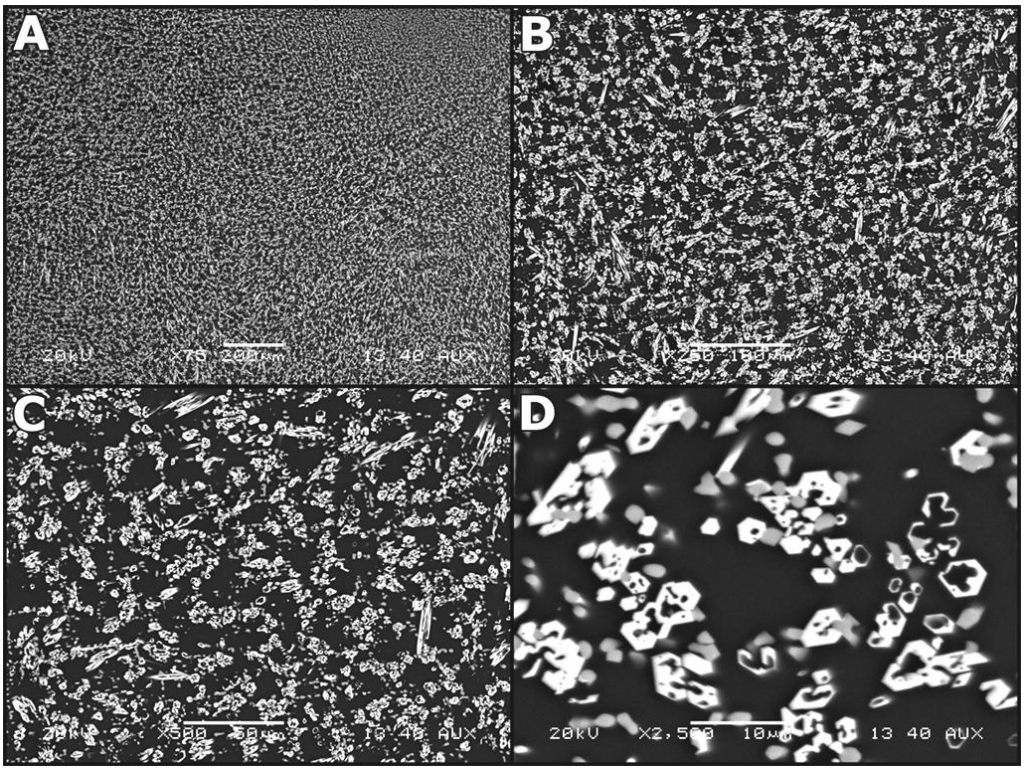

Figure 6. Back-scattered electron imaging micrographs of sample GC-Mo-6.25 (Option 2) glass ceramic with detail on crystals perpendicular to image

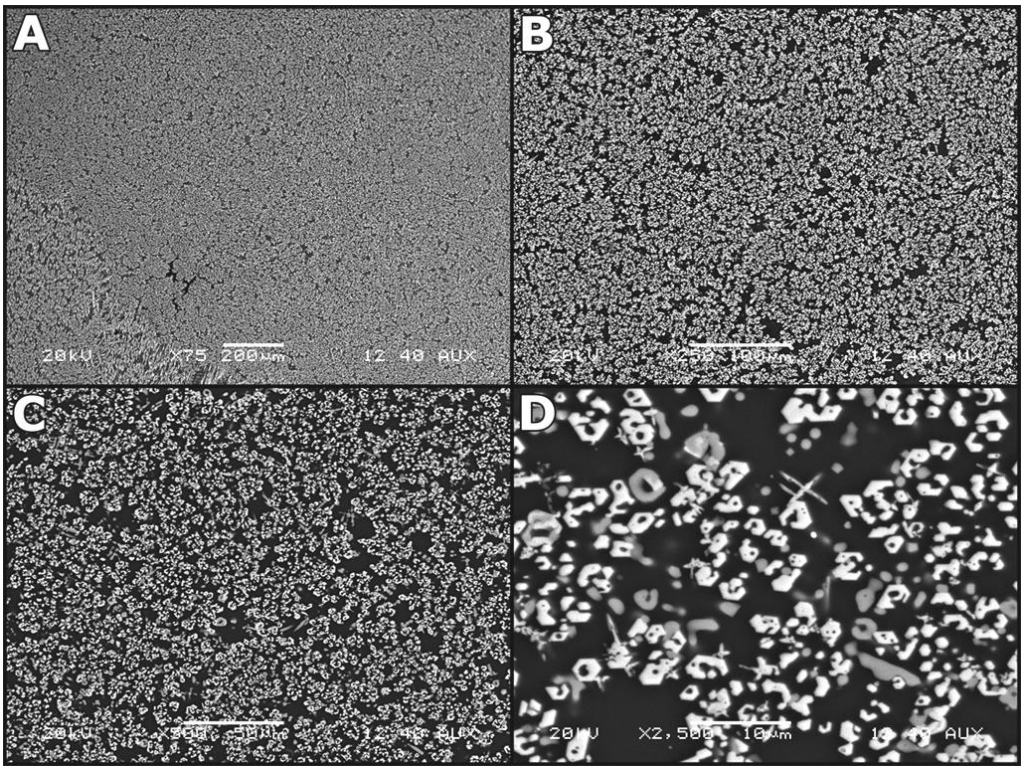

Figure 7. Back-scattered electron imaging micrographs of sample GC-Mo-6.94 (Option 2) glass ceramic with detail on crystals perpendicular to image

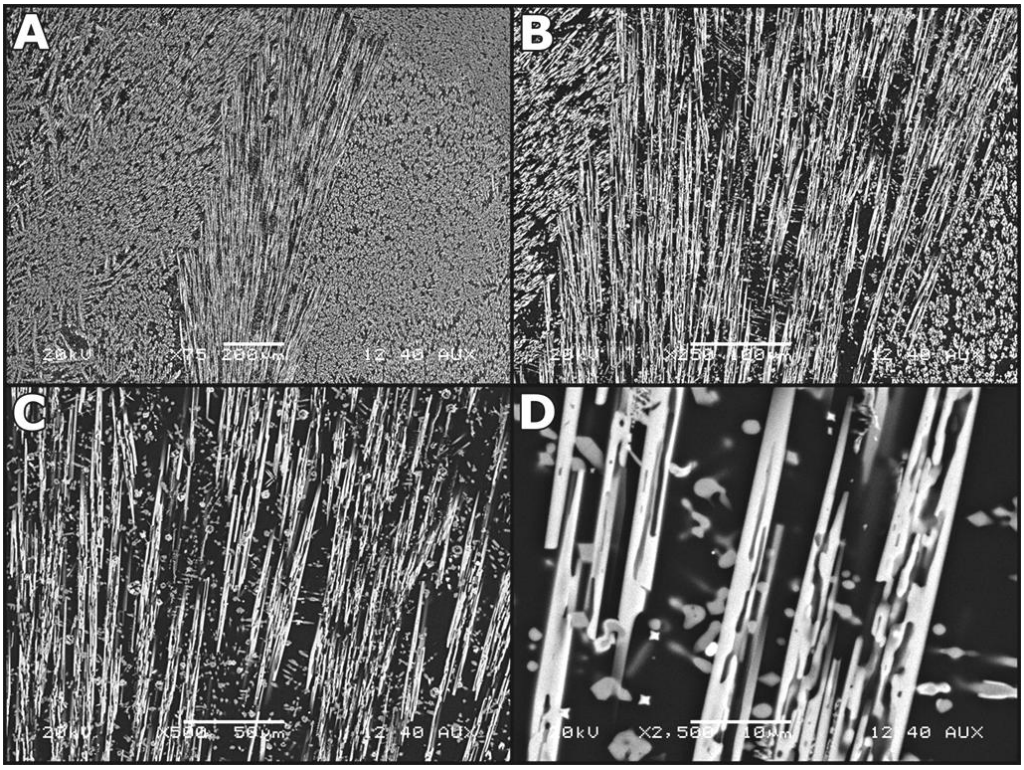

Figure 8. Back-scattered electron imaging micrographs of GC-Mo-6.94 (Option 2) glass ceramic with detail on crystals parallel to image

4.1.3 XRD

The X-ray diffraction patterns collected for the Option 1 and 2 glass ceramics are quite complex because of the multiple phases and high number of reflections in the patterns. In addition, the phases formed are not exact matches to phases found in the ICCD and ICSD databases. The chemistry is more complex than those given in the databases because multiple rare earths and alkaline earths are present in each of the crystalline phases. This leads to small changes in peak locations and intensities. The results of the quantitative XRD analysis are given in Table 7 in terms of mass%. A small but known amount of SRM 674B, rutile (TiO_2), was spiked into each sample to calibrate the 2θ scale and normalize the refined concentrations.[11] The use of an internal standard is required to obtain quantitative results on the concentration of the glass phase in the samples.

The XRD identified additional phases that were not observed by SEM and EDS: RE-borosilicates and two forms of Ba-Al-silicates, celsian and hexacelsian. Borosilicates cannot be identified with EDS analysis because it is insensitive to elements lighter than carbon. Celsian and hexacelsian are chemically identical, but distinguishable with XRD.

Some trends were observed in the XRD data. Rare earth-borosilicate crystals form at low waste loadings whereas oxyapatite forms at higher waste loadings for both Option 1 and 2 glass ceramics. Alkali and alkaline earths form the following crystalline phases in Option 1 glasses: pollucite, celsian, and hexacelsian. However, the concentrations of alkali and alkaline earths are too low to form the same phases in Option 2 glass ceramics at the waste loadings currently being explored. Cerianite and Re-aluminate form as minor phases in some of the Option 1 and/or 2 glass ceramics.

Table 7. Phase assemblage for the Option 1 and 2 glass ceramics by X-ray diffraction, mass%

ID	GC-10B	GC-4-HT	GC-Mo-5.86	GC-Mo-6.25	GC-Mo-6.94
Combined Waste Streams Option	Option 1	Option 1	Option 2	Option 2	Option 2
Heat treatment	2-step HT	-3°C/min	slow cooled	slow cooled	slow cooled
oxyapatite		30	2	21	23
Cerianite		4	1	0	2
$Gd_3(BSiO_6)(SiO_4)$	14	17	17	3	
$La_5(Si_2BO_{13})$		6			
$La_{1.4}Al_{22.6}O_{36}$		4			
Hexacelsian	11	35			
Celsian	7				
Pollucite	11				
Powellite			8	10	9
Glass	57	4	72	66	66
Total	100	100	100	100	100

4.1.4 Dilatometry

Dilatometry was done to determine the material expansion as a function of temperature and to determine T_g and T_d for select Option 1 and 2 glass ceramics. Each sample was measured at a heating rate of 2°C/min from 30°C up to a maximum of 1000°C or the point at which deformation resulted in an overall negative "expansion" result of at least 0.05%, whichever occurred first.

The Option 1 glass ceramic selected was GC-4 (Figure 9). Sample GC-4 shows a very linear expansion as a function of temperature that is indicative of a ceramic material, with no sign of a T_g or T_s, which indicates that if there is a remaining glass phase, it is below the percolation threshold and no longer has an effect on the bulk property. It is fairly safe to assume that sample GC-4 can be modeled based on the thermal stability of its crystalline assemblage.

Two Option 2 glasses, GC-Mo-6.25 and GC-Mo-6.94, were selected for dilatometry, with the results shown in Figure 10. Both samples have a noticeable T_g at 568°C and 562°C, respectively. However, despite this fact, both samples continue to expand with increasing temperature well beyond the expected softening point for a glass up to a temperature of ~950°C. Again, the crystalline structure in the Option 2 glass ceramics have drastically increased the temperature at which negative expansion occurs in comparison to glasses developed for the same combined waste streams. The long, needle-shaped crystals observed in the Option 2 glass ceramics likely have the largest impact on the overall structure of the glass ceramic and result in a high resistance to flow at temperatures well above T_g. Note that for the Option 2 glass ceramic, long-term heat treatments above T_g are needed to track crystallization as a function of time to ensure that long term exposure to elevated temperature does not create a less durable phase.

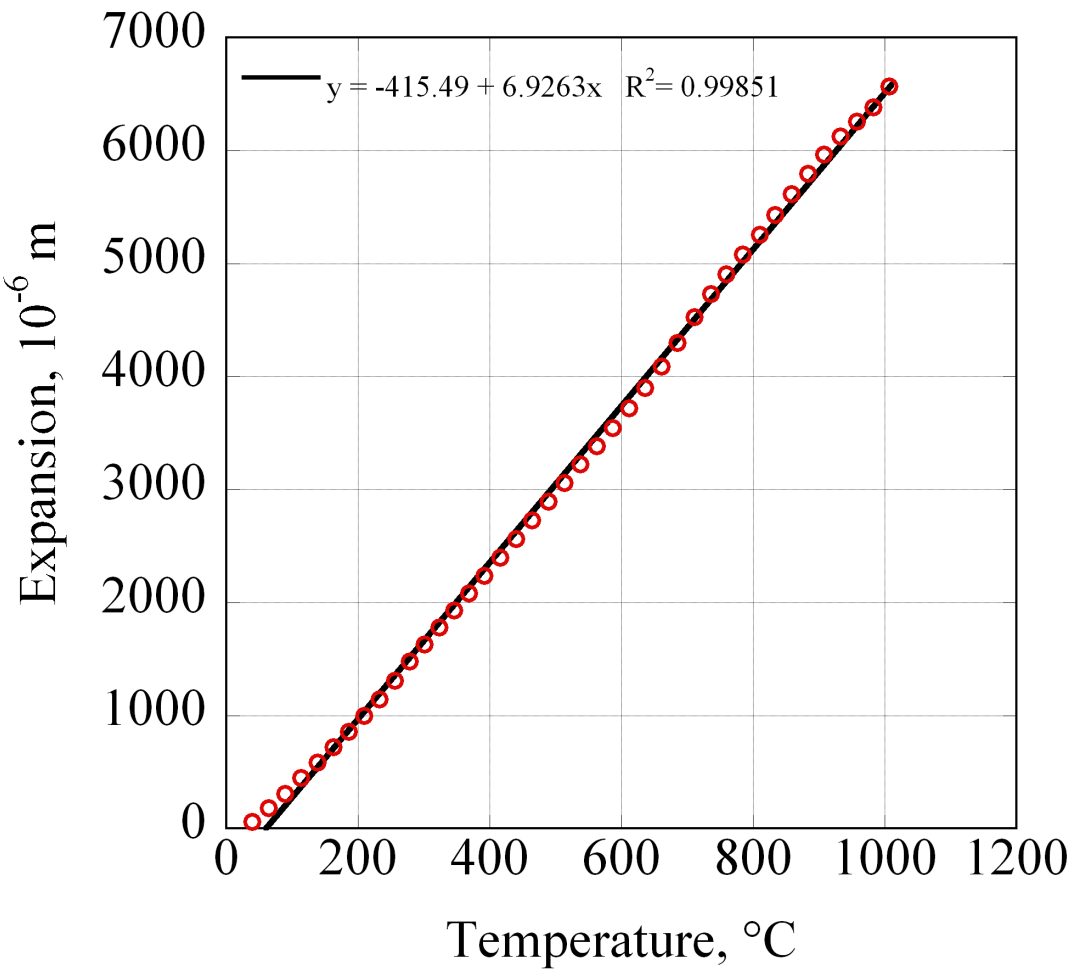

Figure 9. Expansion as a function of temperature for sample GC-4, Option 1 glass ceramic, at a heating rate of 2°C/min from 30°C to 1000°C

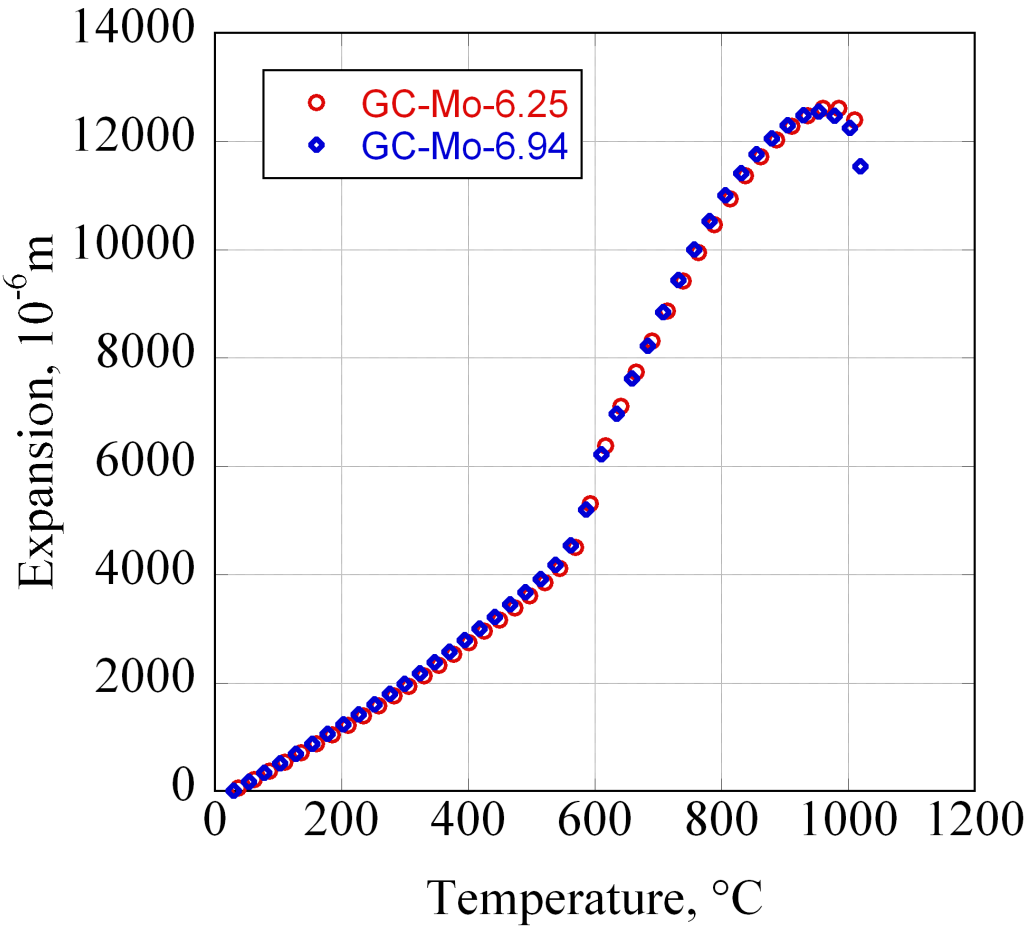

Figure 10. Expansion as a function of temperature for Option 2 glass ceramics at a heating rate of 2°C/min from 30°C to 1000°C

4.1.5 TEM

Figure 11 shows plan-view TEM image obtained from pristine GC-4 sample. In Figure 11, there are four oxide crystalline phases in GC-4 based on EDS spectrums: (1) Al-Sr oxide, (2) Si-Al-Ba/Cs oxide, (3) Si-Ce-Ln oxide (Ce/Nd silicate), (4) Si-Ba-Al oxide. These results are consistent with the SEM/EDS results discussed in 4.1.2.1.

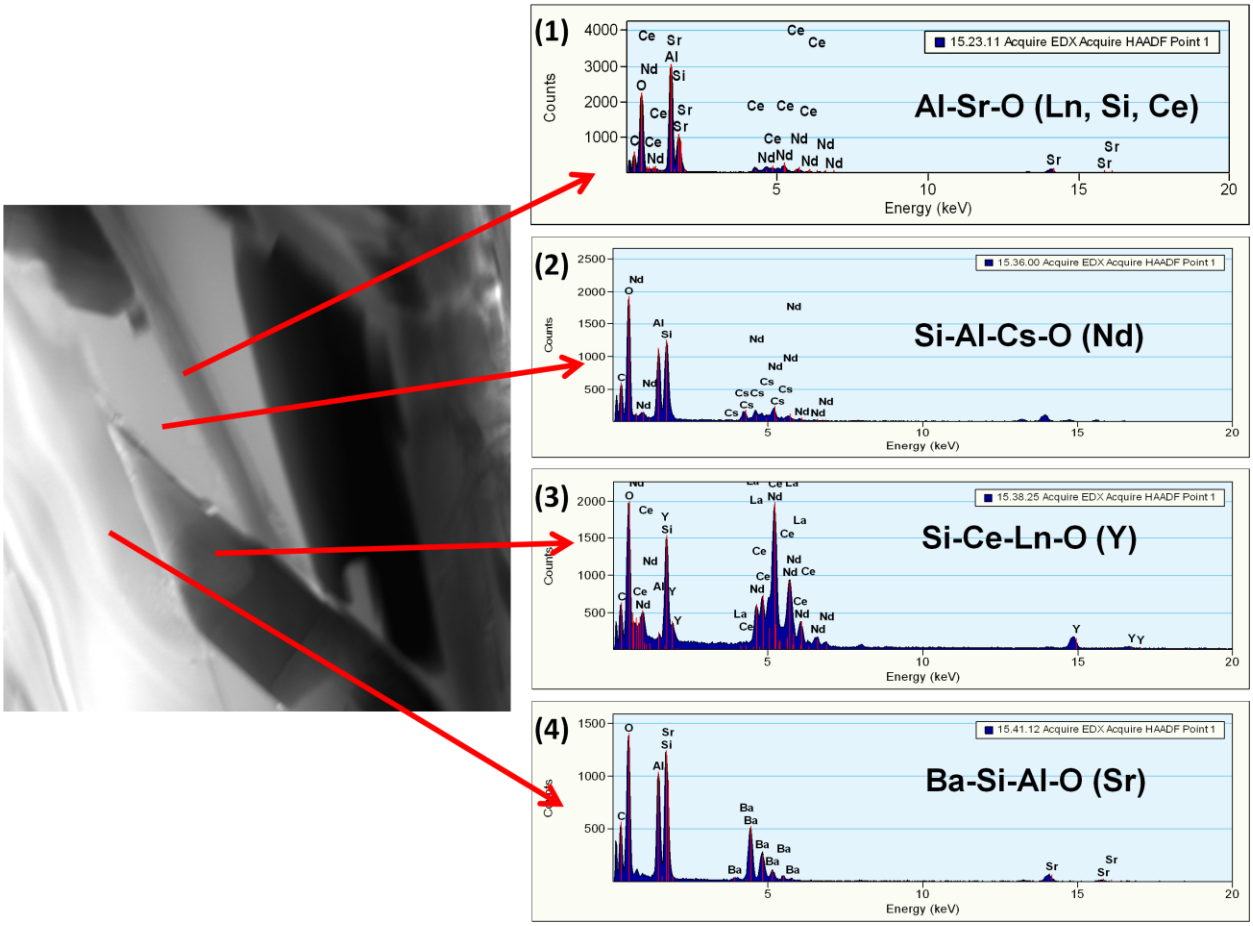

Figure 11. Plan-view TEM image and EDS spectrums of pristine GC-4 sample

4.1.6 Ion Beam Irradiation

Samples GC-4 and Mo-6.94% were subjected to 3 MeV proton, 5 MeV alpha, and 300 keV electron beam irradiation at different temperatures to study the radiation damage tolerance of the glass ceramic waste forms. The irradiated samples were characterized by XRD, SEM and TEM to identify any microstructural changes induced by irradiation.

The Monte Carlo program "The Stopping and Range of Ions in Matter" (SRIM) [12] was used to estimate energy loss/radiation dose in proton and alpha irradiated GC-4. Because of the multiple crystalline phases in GC-4 sample, we used SiO_2 as the target materials in SRIM simulation. A threshold displacement energy of 40 eV was used for all target elements (this was arbitrary). Figure 12 shows the results of a SRIM simulation for SiO_2. The range of 3 MeV H^+ in SiO_2 is ~80 um and the peak radiation dose corresponds to 0.2 GGy with a fluence of 1×10^{16} ions/cm^2. The range of 5 MeV He^+ in SiO_2 is ~20um and the peak radiation dose corresponds to 8.3 GGy with a fluence of 1×10^{17} ions/cm^2.

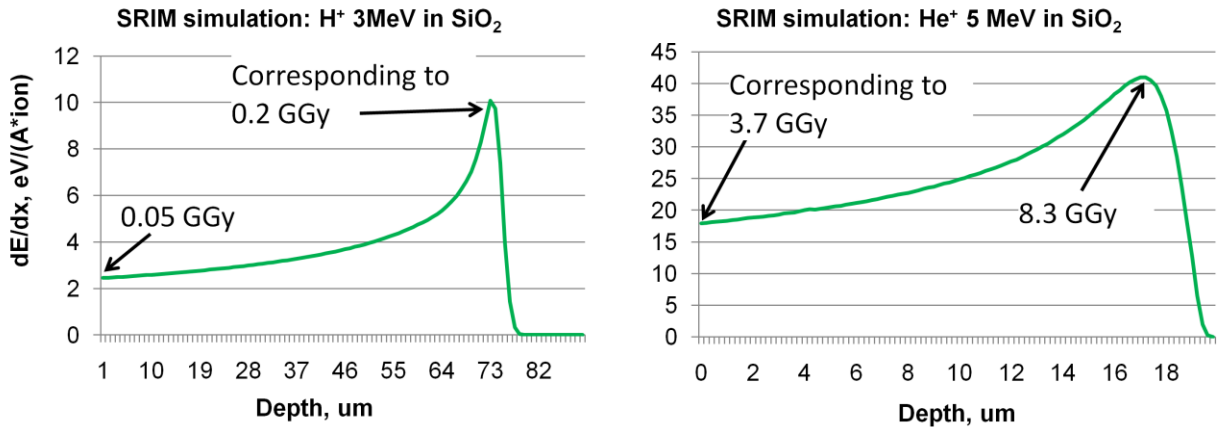

Figure 12. SRIM simulation results show energy loss and radiation dose of 3 MeV H^+ ion (left) and 5 MeV He^+ (right) for SiO_2 as function of ion penetration depth

As mentioned previously, the X-ray diffraction patterns from samples GC-4 and Mo-6.94% are quite complex because of the multiple phases and high number of reflections in the patterns. The XRD observations reveal that irradiation leads to small changes in peak locations and intensities in both samples. Figure 13 shows XRD patterns from the GC-4 sample before and after 3 MeV proton irradiation to a fluence of 1×10^{16} ions/cm^2 at 230°C. For the irradiated GC-4 sample, these XRD patterns do not show any amorphous features, while the XRD observation suggests that the proton irradiation induces texturing of Ce/Nd silicate phase. Figure 14 shows diffraction patterns obtained from the GC-4 sample before and after 5 MeV alpha irradiation to a fluence of 1×10^{17} ions/cm^2 at room temperature, showing structural evolution similar to the proton irradiated GC-4 sample.

For the Mo-6.94% sample irradiated with 3 MeV protons to a fluence of 1×10^{16} ions/cm^2 at 230°C, XRD patterns in Figure 15 reveal there is no appreciable changes before and after irradiation. It is noteworthy that, despite the apparent texturing of some of these crystalline phases (Ce/Nd silicate), no amorphization was observed in the irradiated GC-4 and Mo-6.94% samples in this electron energy loss regime, up to a maximum ion dose of 8.3 GGy.

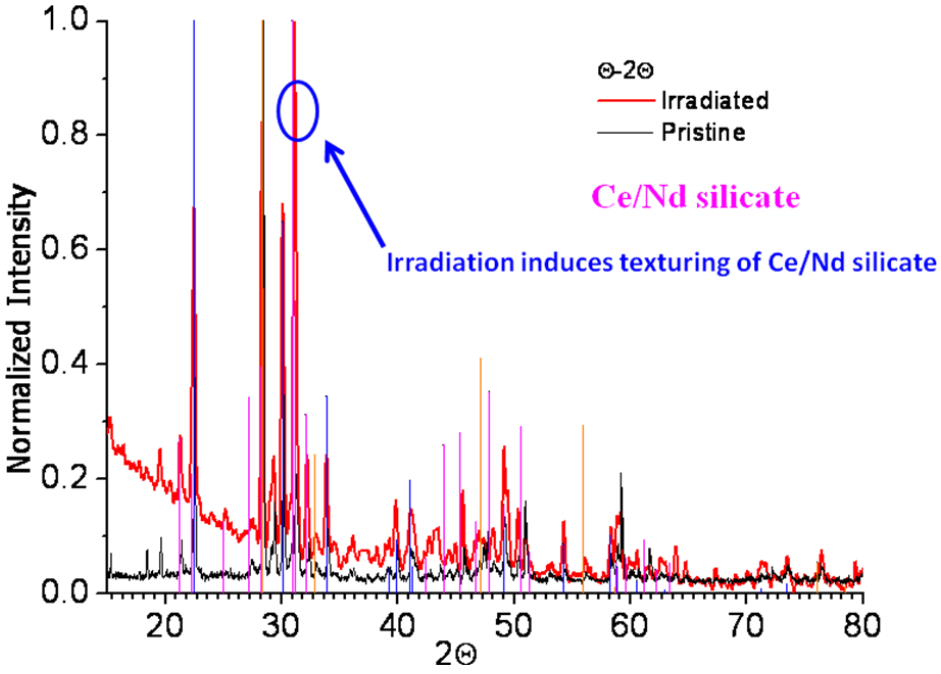

Figure 13. Results from XRD for GC-4 sample before and after 3 MeV proton irradiation with a fluence of 1×10^{16} ions/cm^2 at 230°C

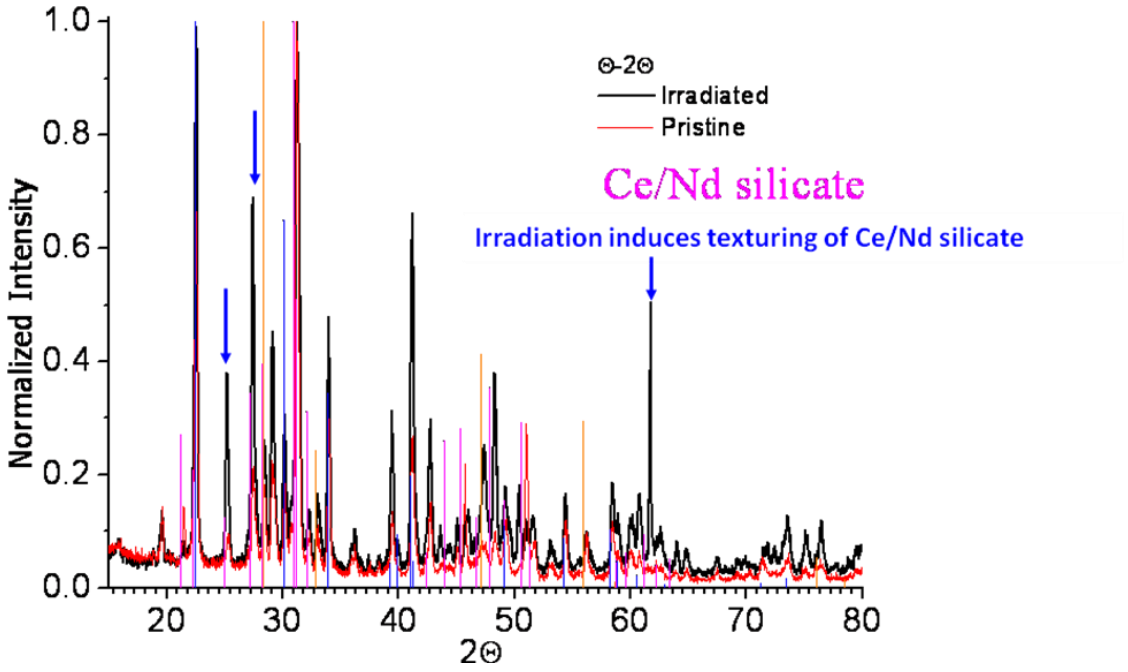

Figure 14. Results from XRD for GC-4 sample before and after 5 MeV alpha irradiation with a fluence of 1×10^{17} ions/cm^2 at room temperature

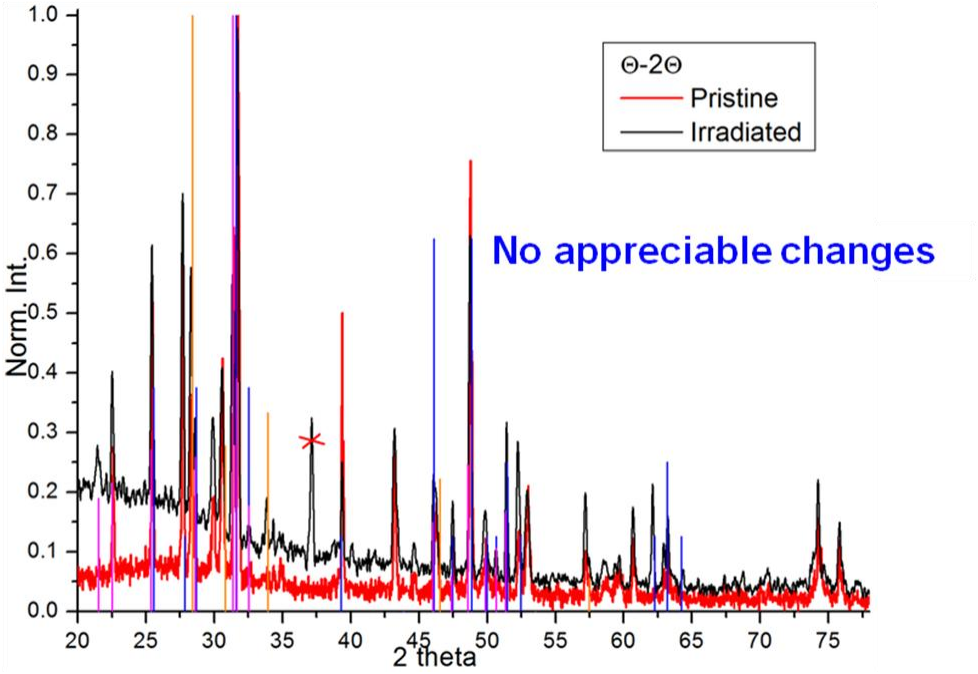

Figure 15. Results from XRD for Mo-6.94% sample before and after 3 MeV proton irradiation with a fluence of 1×10^{16} ions/cm^2 at 230°C

To examine the electron beam irradiation-induced microstructural evolution of GC-4 sample, we performed 300 keV electron beam irradiation on this sample. Figure 16 shows high resolution TEM images for Ce/Nd silicate phase before (left) and after (right) electron radiation, along with the fast Fourier transformation (FFT) diffractogram. Lattice fringes in the red circle area in Figure 16 reveal that the irradiated area of Ce/Nd silicate phases possess a different structure compared to the unirradiated area. The FFT analysis suggests that this is due to a crystalline-to-crystalline phase transformation. A Cs/Al silicate phase in the GC-4 sample, however, shows no evidence of microstructural changes after electron irradiation (Figure 17). Without a faraday cup, we could not measure the exact electron fluence during the electron beam irradiation, so our electron irradiation results should be treated as preliminary and qualitative. However, TEM observations for these two crystalline phases in GC-4 sample are consistent with our previous XRD results.

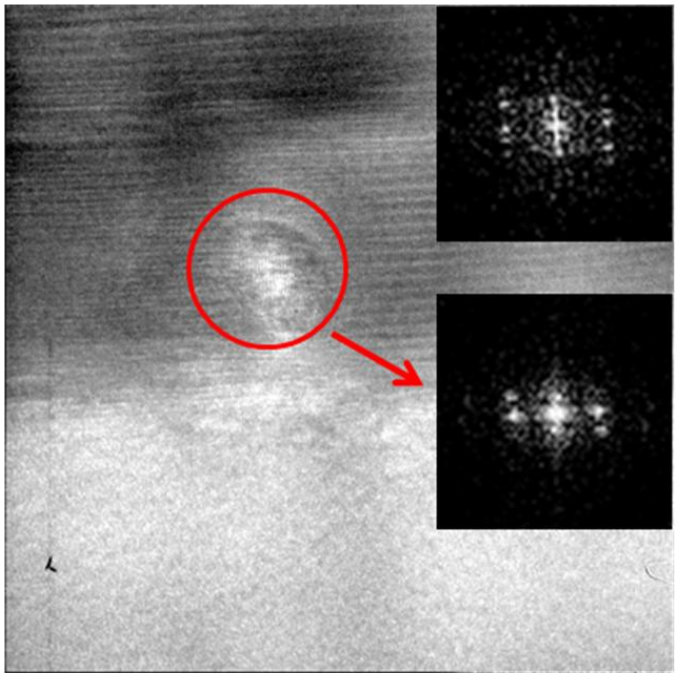

Figure 16. High resolution TEM images for Ce/Nd silicate phase before (left) and after (right) electron radiation, also shown are diffractograms obtained by fast Fourier Transforms (FFT) from different areas

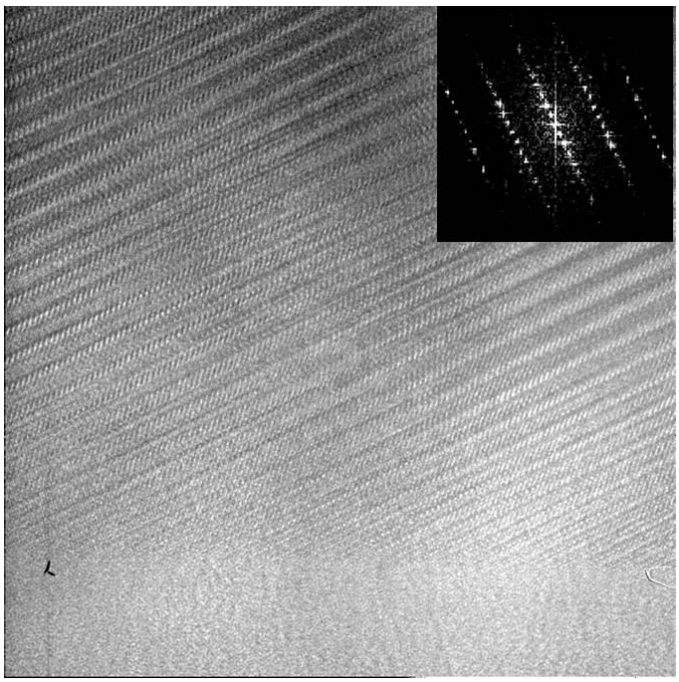

Figure 17. High resolution TEM image for Cs/Al silicate phase under electron radiation, also shown are diffractogram obtained by FFT

5. Conclusions/Future Work

Glass ceramics are being explored as an alternative waste form for glass, the current baseline, for treatment of CS+LN or CS+LN+TM fission-product waste streams. The four main reasons for exploring glass ceramics are:

- Glass ceramics offer increased solubility of troublesome components in crystalline phases as compared to glass, leading to increased waste loading.
- The crystalline network formed in the glass ceramic results in higher heat tolerance than glass.
- Glass ceramics maintain most if not all of the composition flexibility that makes glass waste forms so attractive.
- These glass ceramics are designed to be processed by the same melter technology as the current baseline glass waste form. It will only require the addition of controlled canister cooling for crystallization into a glass ceramic waste form.
- The waste form will be up to 50% lower surface area than a typical HLW glass (in a canister) because of the annealing process (controlled cooling) used to achieve a glass ceramic.

This was the first full year of exploring glass ceramics for the Option 1 and 2 combined waste stream options. We have shown that dramatic increases in waste loading are achievable by designing a glass ceramic waste form in comparison to the current baseline glasses. Table 8 shows the upper limits for heat, waste loading (solubility), and the decay time needed before treatment can occur for glass and glass ceramic waste forms. The improvements are significant for both combined waste stream options in terms of waste loading and decay time. For Option 1, glass ceramics show an increase in waste loading of 15 mass% and a reduction in required decay time of 24 years before treatment. A decay time of 50 years is close to the expected age of the fuel that will be reprocessed based on current estimates. Option 2 shows a 2× to 2.5× increase in waste loading with decay times of only 45 years. Note that for Option 2 glass, the required decay time before treatment is only 35 years because of the waste loading limits related to the solubility of MoO_3 in glass. These glass ceramics are not optimized, but already they show the potential to dramatically reduce the amount of waste generated while still utilizing the proven processing technology used for glass production.

Table 8. Comparison of baseline glasses to current glass ceramic waste forms

Option 1	Glass [1]	Glass Ceramic	
Heat Limit, °C	700	1250	1250
Waste Loading, %	45	55	60
Required Decay, y	76	48	52

Option 2	Glass [1]	Glass Ceramic	
Heat Limit, °C	500	950	950
Waste Loading, %	20	40	50
Required Decay, y	35	36	45

Option 1 = CS+LN, Option 2 = CS+LN+TM

Initial studies of TEM characterization reveal the complexity in crystal structures in glass ceramic waste forms. Additional studies in this area are needed:

- Electron Energy Loss Spectroscopy (EELS) technique associated with TEM will be used to identify boron distribution in our glass ceramic samples
- Lattice parameters will be calculated from high resolution TEM images. Combining with XRD data, we should be able to identify the multiple phases chemically and structurally.

Preliminary irradiation stability studies show very promising radiation tolerance in our glass ceramic samples, since no amorphization was observed under irradiation. More irradiation stability tests will be performed at higher radiation doses and different temperature range with electron (TEM, electron accelerator), light ions (alpha, proton), and dual beam (light high energy ions combined with heavy low energy ions).

The FY 2010 effort spent exploring silicate-based glass ceramics for immobilizing Option 1 and 2 combined waste streams showed that treatment of all three oxide waste streams CS+LN+TM combined into a single waste form is very viable in terms of waste form volume and overall cost. Significantly more so than a glass only waste form. From a reprocessing operations standpoint, this would be the simplest and most cost effective immobilization option. For this reason, next year's efforts will focus on further development of Option 2 glass ceramics as the treatment of all three waste steams combined in a single waste form.

The next year work will focus on:

- The multiphase glass ceramics have unique crystalline phases that require full characterization chemically and structurally.
    - Techniques may include FIB-TEM, neutron diffraction, electron microprobe, and micro XRD. Techniques will focus on gathering high quality diffraction data on the waste form and individual phases (if possible). Obtaining qualitative (at a minimum) or quantitative concentrations of boron in the crystalline phases.
- Evaluate performance of the multi-phase glass ceramics by static and/or flow through dissolution test.
- Reformulate a new series of glass ceramics to improve performance and waste loading in multiphase glass ceramics. The remaining glass composition is usually the culprit of poor performance. Thus chemistry changes will be made to help tailor the remaining glass composition.

The following optional task will be pursued if time and budget allow:

- Synthesize powellite, oxyapatite, and RE-borosilicate crystalline phases for radiation damage testing. Single phases provide more flexibility in radiation damage testing.
- Evaluate the performance of individual crystalline phases by static and/or flow through dissolution test, once they are fully characterized.
- Identify and test a method for irradiation of a glass ceramic on a large enough scale for dissolution testing, followed by static or flow through dissolution testing.
    - Identify a gamma and or beta source(s) for the irradiation
    - Perform single pass flow through or static dissolution testing of powders or monolith

6. References

1. Gombert, II, D., Carter, J., Ebert, W., Piet, S., Trickel, T., and Vienna, J., "A Trade Study for Waste Concepts to Minimize HLW Volume," *Scientific Basis for Nuclear Waste Management XXXII*, p 53-64, 2009.
2. Crum, J. V., Billings, A. L., Lang, J., Marra, J. C., Rodriguez, C., Ryan, J. V., and Vienna, J. D., Baseline Glass Development for Combined Fission Products Waste Streams, AFCI-WAST-WAST-MI-DV-2009-000075, 2009
3. Kim, D-S., Peeler, D. K., and Hrma, P., "Effects of Crystallization on the Chemical Durability of Nuclear Waste Glasses," *Ceram. Trans.* 61, 177-185, 1995
4. Li, H., Vienna, J. D., Hrma, P., Smith, D. E., and Schweiger, M. J., "Nepheline Precipitation in High-Level Waste Glasses – Compositional Effects and Impact on the Waste Form Acceptability," *Mat. Res. Soc. Proc.* 465, 261-268, 1997
5. Riley, B. J., Hrma, P., Rosario, J., and Vienna, J. D., "Effect of Crystallization on High-Level Waste Glass," *Ceram. Trans.* 132, 257-265, 2002
6. Ryan, J. V., Buck, E. C., Chun, J., Crum, J. V., Riley, B. J., Strachan, D. M., Sundaram, S. K., Turo, L. A., and Vienna, J. V., Alternate Waste Forms: Aqueous Processing, AFCI-WAST-PMO-MI-DV-2009-000360, 2009
7. "Glass Batching and Melting," Pacific Northwest National Laboratory (PNNL), Richland, WA, Report No. Technical Procedure GDL-GBM, Rev. 3.
8. Cheary, R. W., Coelho, A. A., and Cline, J. P., "Fundamental Parameters Line Profile Fitting in Laboratory Diffractometers," *J. Res. Natl. Inst. Stand. Technol.* 109, 1-25, 2004
9. Waste/Storage Form Baseline-Fission Products & Lanthanides, A. L. Youchak-Billings, J. V. Crum, J. C. Marra, B. J. Riley, J. D. Vienna, and A. Edmondson, GNEP-WAST-PMO-MI-DV-2008-000151, 2008
10. Caurant D, Majerus O, Fadel E, and Lenoir M., "Effect of Molybdenum on the Structure and on the Crystallization of SiO2–Na2O–CaO–B2O3 Glasses," J. Am. Ceram. Soc., 90 [3] 774–783 (2007)
11. SRM 674b; *X-ray Power Diffraction Intensity Set for Quantitative Analysis by X-Ray Diffraction*; National Institute of Standards and Technology; Department of Commerce: Gaithersburg, MD (2007)
12. J.F. Ziegler, J.P. Biersack, U. Littmark, The Stopping and Range of Ions in Solids, Pergamon Press, New York, 1985.